Wetting and Interfacial Properties of Water Nanodroplets in Contact with Graphene and Monolayer Boron–Nitride Sheets

Hui Li and Xiao Cheng Zeng*

Department of Chemistry and Nebraska Center for Materials and Nanoscience, University of Nebraska, Lincoln, Nebraska, 68588

ABSTRACT

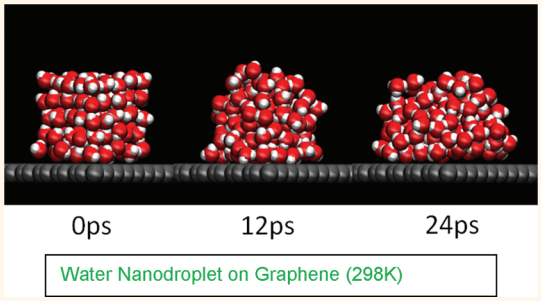

Born–Oppenheim quantum molecular dynamics (QMD) simulations are performed to investigate wetting, diffusive, and interfacial properties of water nanodroplets in contact with a graphene sheet or a monolayer boron–nitride (BN) sheet. Contact angles of the water nanodroplets on the two sheets are computed for the first time using QMD simulations. Structural and dynamic properties of the water droplets near the graphene or BN sheet are also studied to gain insights into the interfacial interaction between the water droplet and the substrate. QMD simulation results are compared with those from previous classic MD simulations and with the experimental measurements. The QMD simulations show that the graphene sheet yields a contact angle of 87°, while the monolayer BN sheet gives rise to a contact angle of 86°. Hence, like graphene, the monolayer BN sheet is also weakly hydrophobic, even though the BN bonds entail a large local dipole moment. QMD simulations also show that the interfacial water can induce net positive charges on the contacting surface of the graphene and monolayer BN sheets, and such charge induction may affect electronic structure of the contacting graphene in view that graphene is a semimetal. Contact angles of nanodroplets of water in a supercooled state on the graphene are also computed. It is found that under the supercooled condition, water nanodroplets exhibit an appreciably larger contact angle than under the ambient condition.

KEYWORDS: contact angle · water nanodroplet · graphene · boron nitride monolayer · quantum molecular dynamics simulation · supercooled water

The interactions between water and material surfaces are manifested in the wetting properties of the material, as well as in many interfacial phenomena in a variety of chemical, biological, and technological systems.[1] For example, interfacial water can act as a lubricant in water–clay systems,[2,3] or supplies attractive interactions among hydrophobic groups of proteins or lipid bilayers.[4–7] Moreover, understanding physical behavior of the interfacial water has important implications for the design of nanostructured devices such as those built upon carbon nanotubes (CNTs) or graphene nanoribbons. This is because all nanostructured devices possess large surface-to-volume ratios. As a consequence, interfacial water, if present, may significantly affect functions of these devices. Certain nanostructured devices can be utilized as sensors and, typically, these sensors are either exposed to the open air or immersed in an aqueous environment.[8] To date, the wetting behavior of water on carbon CNTs and graphene/graphite surfaces has been studied by many researchers, either experimentally[9–16] or theoretically.[17–21] These studies have shown that the wetting and dynamical properties of water can be strongly dependent on the chemical composition[22–28] and microstructure[29–34] of the contacting surfaces.

For atomically flat and homogeneous surfaces, such as graphene sheets, their wettability (or hydrophilicity) is mainly determined by the chemical properties of the surfaces.[1] In turn, the large dipole moment associated with the water molecules may also significantly affect electronic properties of contacting surfaces.[20] Graphite is known to be weakly hydrophobic with an apparent water contact angle in the range of 80–90°.[10] However, on epitaxial graphene grown on silicon carbide, a reported experimental contact angle is 92.5°.[15] Another recent study of water droplets on thin films of graphene shows that the contact angle can be as large as 127°.[16] It is also known that one-dimensional (1D) CNTs have low solubility in water due in part to their high surface curvatures.[11]

* Address correspondence to xzeng1@unl.edu.

Received for review November 30, 2011 and accepted February 14, 2012.

Published online February 22, 2012
10.1021/nn204661d

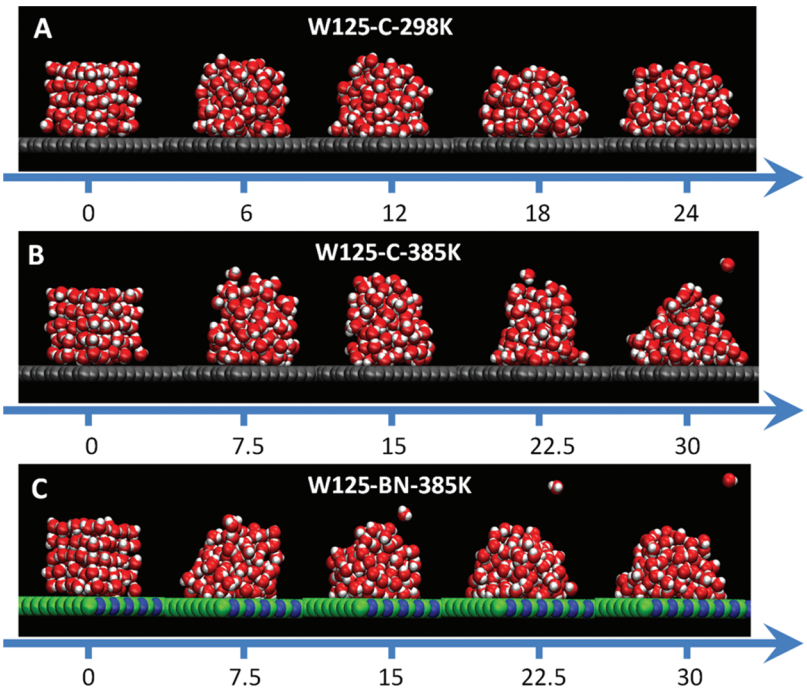

Figure 1. Snapshots of a water nanodroplet during the time evolution (in unit of ps) of the wetting process on a graphene sheet at (A) 298 K and (B) 385 K, and (C) on the BN sheet at 385 K. Color code for elements: O, red; H, white; C, gray; B, green; and N, blue.

1D boron–nitrite (BN) naonotubes and 2D hexagonal BN monolayers are structural analogues of CNTs and graphene sheets, respectively. Like CNTs and graphene, the BN nanostructures have also received considerable attention particularly owing to their unique properties such as size- and chirality-independent band gap and exceptional resistance to oxidation. Some previous experimental studies have demonstrated that BN thin films exhibit weaker hydrophobicity (or higher wettability) than the graphene sheets, as they yield smaller contact angles of 50–67°[35,36] when in contact with water droplets. Presumably, the higher water wettability for the BN thin films is due to polar nature of B–N bonds. Another important factor that can affect wettability of a surface is the temperature of the system. It is known that supercooled water can exhibit many unusual thermodynamic properties, for example, among others, negative thermal expansion, high isothermal compressibility, and isobaric heat capacity.[37] However, few studies have been devoted to the wettability (or hydrophilicity) of surfaces when the surfaces are in contact with water droplets under the supercooled conditions.

Classical MD simulations have been widely used to study the wetting properties of graphite surfaces since the pioneer work of Rahman and Stillinger.[38] Various water models have been examined, including simple point charge (SPC and SPC/E),[39] TIPS,[40] TIP3P,[41] TIP4P,[41] and TIP5P[42] models. However, it has been shown that structure of the water/graphite interface can be very sensitive to the water model selected.[43] For water–CNT systems, it has been shown that the diffusion constant of water confined to CNT is larger along the tube axis than that of bulk water when the flexible SPC model is used,[44–47] whereas much lower mobility of water is found when the rigid SPC model is used.[48–51] All these results suggest that the interfacial properties predicted based on classical MD are semiquantitative in view of the observed model dependence. Compared to those of classic MD, QMD simulations are more reliable because the intermolecular forces are computed based on the first principle rather than an empirical force field. Moreover, quantum calculations are more accurate in describing the polarization interaction, many-body effects, and hydrogen bonding interaction. As an example, the diffusive property of confined water between two graphene sheets has been investigated by Cicero *et al.* using QMD simulations.[18] They demonstrated the existence of a thin, interfacial liquid layer (~5 Å) whose microscopic structure and thickness are independent of the distance between confining graphene sheets. They also found that the properties of the hydrogen-bonding network are very similar to those of the bulk water outside the interfacial region.

In this article, we report QMD simulations of wetting, diffusive, and interfacial properties of water nanodroplets in contact with graphene and monolayer BN sheets. The computed wetting properties of graphene and BN surfaces allow us to examine effects of nonpolar C–C bonds vs polar B–N bonds on the water/substrate interaction. The wettability of the two sheets can be characterized by the magnitude of the contact angle of a water nanodroplet. Microstructures of water

nanodroplets, the mean squared displacement (MSD) of water molecules, vibration spectra, and water reorientation time-correlation function are computed to gain insights into the physical behavior of water near the substrates. We have found that the diffusivity of water and the contact angle of water nanodroplets near the two sheets are very similar to each other, contrary to the conventional view that the graphene surface is more hydrophobic than the BN surface. In addition, for the first time, wetting properties of the graphene when in contact with a water droplet under the supercooled condition are investigated. Diffusivity of water molecules under the supercooled condition is compared with that under the ambient condition. The graphene sheet appears to be slightly more hydrophobic compared to that under the ambient condition.

RESULTS AND DISCUSSION

The QMD simulations (see Computational Model and Method) of three droplet-substrate systems are performed at two temperatures, 298 and 385 K. Previous density-functional theory (DFT) based QMD simulations have shown that the freezing point of DFT water is significantly higher than 273 K, ~360 K if the BLYP-D functional is used (see Method). Hence, the 298 K considered here is actually a supercooled temperature for the water nanodroplet, while the 385 K simulation is likely close to the ambient condition.

Wetting Properties and Contact Angles. Snapshots of a water nanodroplet during the spreading either on a graphene sheet or on a BN sheet are shown in Figure 1. QMD trajectories for the droplet−graphene system at 298 K are shown in the Supporting Information video 1. Both the graphene and BN surfaces exhibit partial wetting behavior (or weakly hydrophobic behavior) since the water droplet does not spread over the entire graphene or BN sheet in the simulation systems. As shown in Figure 1, after 10 ps simulation, the initial cubic configuration of water droplet turns into a hemispheric configuration. This equilibration process is much faster at 385 K than at 298 K. In the simulation at 385 K, a few water molecules are observed to depart from the droplet and become vapor molecules. However, this phenomenon is not observed in the simulation at 298 K. During the first 10-ps simulation, it can be seen that the peak height of the water droplet at 385 K is slightly higher than that at 298 K, suggesting the wettability of the graphene is slightly lower when the water droplet is in the supercooled state.

The contact angle is defined as the angle between the substrate and a tangential line of the droplet surface, where the tangential line must passes through a 3-phase contact point while the plane made by the tangential line and its projection to the substrate must pass the center of the droplet. The computational method for calculating the contact angle is similar to

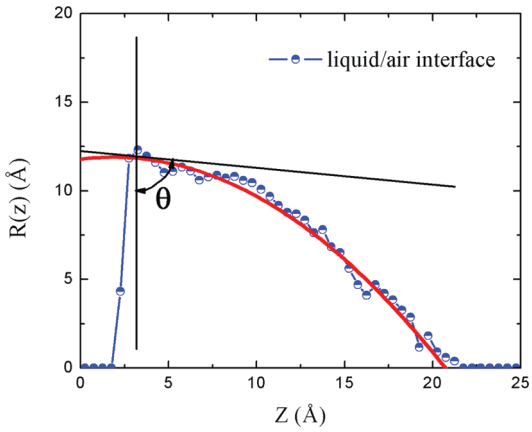

Figure 2. Illustration of the contact-angle measurement based on QMD simulations. The blue line denotes to the liquid/air interface (averaged over the last 10 ps) for the water droplet on the monolayer BN sheet; the red curve marks the fitted surface of the water droplet. The contact angle (θ) is the angle between the (black) tangent line and the *xy* plane (marked by the vertical black line). Note that the *xy* plane is located about a molecular layer of water higher than the contacting surface of the BN substrate ($z = 0$).

that used in ref 1. As shown in Figure 1 (and Supporting Information, video 1), the systems appear to be fully relaxed within the first 10 ps. We compute the contact angle by using the MD trajectory of the last 10−20 ps. To compute the contact angle, we first define a *z*-axis through the center of mass of the droplet and normal to the substrate. We then divide the system into cubic meshes with each mesh having spatial dimensions of $0.5 \times 0.5 \times 0.5$ Å^3. The average density of water in each mesh is calculated, and all the meshes with water density greater than 0.3 g/cm^3 are recorded. For a selected layer of meshes with nearly equal-density, a circle (in parallel with the substrate) with its center located on the *z* axis is fitted. As such, the radius of the circle is obtained as a function of the height, that is, $R(z)$. It should be noted that for nanodroplets, the molecular volume of water must be taken into account in the curve fitting. In other words, the radius of a water molecule (1.4 Å) should be added to the final values of $R(z)$. Figure 2 shows the density profile of a water droplet on the BN sheet at 385 K. The contact angle (θ) is obtained based on fitting the density profiles by using the function $R(z) = Az^2 + Bz + C$ (see Figure 2). Note also that for nanodroplets, the measured contact angle is sensitive to the height of the plane that represents the contacting surface of the substrate. Here, we define the first peak position of the density profile in the *z* direction as $z = 0$ for the contact-angle measurement. This zero height is about 3.0 Å above the center of the sheets in the *z*-position, and it also marks the *z*-position of the first water layer.

Based on the QMD trajectory from 10 to 30 ps, the measured contact angles of a water nanodroplet on the graphene is ~87° at 385 K, close to the

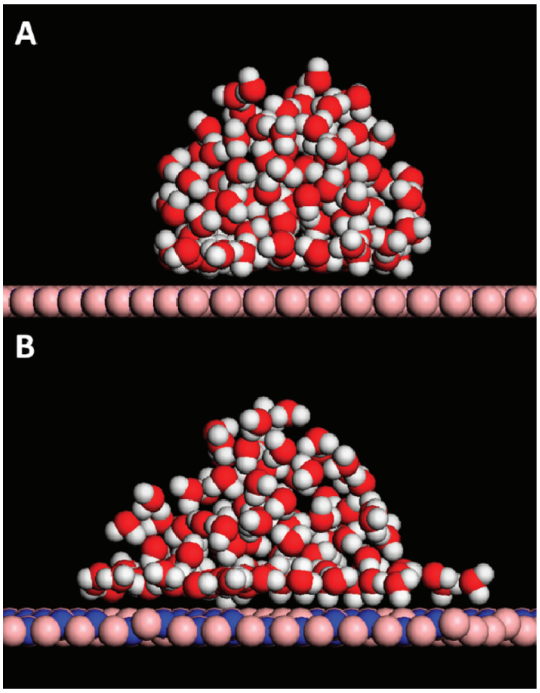

Figure 3. Snapshots of a water droplet on (A) an atomically flat and (B) a wrinkled BN sheet in the end of classical molecular dynamics simulation with a flexible SPC water model.

experimentally measured contact angle of water on the epitaxial graphene grown on silicon carbide (92.5°).[15] The computed contact angle of the water nanodroplet on graphene under the supercooled condition is ~96° at 298 K, about 9° larger than the droplet under the ambient condition. Our simulation suggests that the wettability of a solid surface under the supercooled condition is slightly weaker than under the ambient condition. Surprisingly, the contact angle on a flat BN sheet is 86°, much larger than previously reported experimental values (52° or 67°), implying that the atomically flat monolayer BN sheet has very similar wettability (or hydrophobicity) as the graphene sheet.

In a previous simulation study, it has been shown that the hydrophobicity of a substrate decreases largely with an increase of the surface dipole of the substrate.[1] In our DFT calculation, the electron density fitting gives rise to atomic charges of boron (0.93*e*) and nitrogen (−0.93*e*) for the monolayer BN sheet, resulting in a sizable local dipole moment. To have a better understanding of the wettability or the hydrophobicity of the monolayer BN sheet, we have also performed two independent classic MD simulations using the flexible SPC model of water. The system temperature is controlled at 250 K. In the first MD simulation, a water nanodroplet with the same size as in the QMD simulation is located on a flat and rigid monolayer BN sheet. In the second simulation, some random wrinkles (with vertical amplitude <0.5 Å) are introduced on the monolayer BN sheet. The contact angle of the water droplet on the flat BN sheet is notably larger than that on the wrinkled BN sheet, as shown by the snapshots of the droplets near the end of two simulations (see Figure 3). Clearly, the higher wettability (or weaker hydrophobicity) of the wrinkled BN sheet is due to the appearance of vertical dipoles on the wrinkled BN surface. Our classical MD simulations confirm that only dipoles normal to the substrate can strongly enhance wettability of the substrate. However, in a real-world experiment, it is very difficult to achieve a perfectly flat monolayer BN sheet without any defects. This may be a main reason that the experimentally measured contact angle for water droplets on the BN surface is appreciably smaller than the contact angle computed from the QMD simulation.

Microstructure of Water Nanodroplets and Interfacial Properties. To analyze structures of water nanodroplets on the graphene or BN sheet, we calculate the density distributions of oxygen and hydrogen atoms along the *z* direction normal to the substrate. To this end, we select 36 atoms on the substrate (C atoms on graphene or B and N atoms on BN) around the origin of *z* axis. Thirty-six vertical and identical cylinders are created with their central axis passing through the 36 atoms and with their radius being half of the length of either the C−C or B−N bond. We then count the number of oxygen and hydrogen atoms within each of 36 vertical cylinders during the last 10 ps QMD simulations. The computed density distributions of oxygen and hydrogen for the three droplet−substrate systems are shown in Figure 4. The first and second molecular layers of water next to the substrate can be clearly identified for all three systems. The first and second main peaks (Figure 4) for the droplet−BN system are notably higher than those for the droplet−graphene systems, indicating that the interaction between the BN surface and water is stronger than between graphene and water. Moreover, the height of the second main peak is much lower for the droplet−graphene system at 385 K than it at 298 K, indicating that under the supercooled condition vicinal water becomes structured (or more ordered) in the interfacial region than under the ambient condition.

As shown in Figure 4A,B, in these droplet−substrate systems, the first peak for hydrogen is higher than the first peak for oxygen, but the area under the hydrogen peak is apparently less than twice of the area under the oxygen peak. Between the first and the second peaks for oxygen, small hydrogen peaks can be found, indicating that some water molecules in the first vicinal water layer have their OH bonds pointing toward the droplet side (*i.e.,* not in parallel with the substrate). Because an oxygen atom entails more atomic charge (in magnitude) than a hydrogen atom, the net charge next to the substrate on

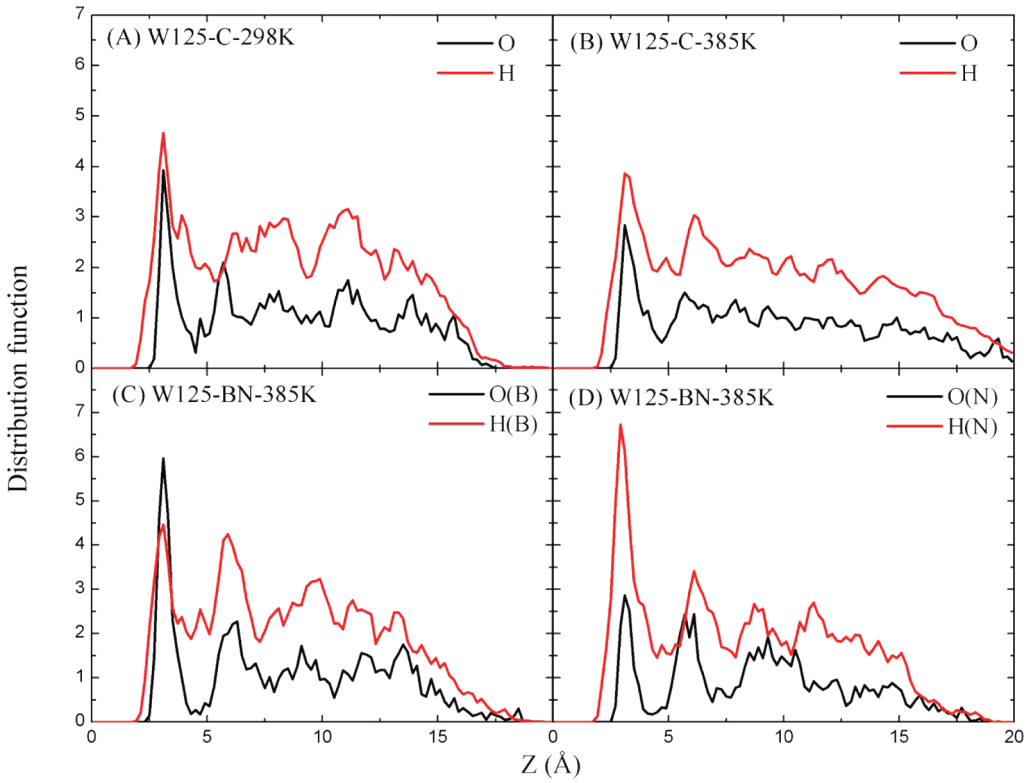

Figure 4. Density distribution (arbitrary unit) of oxygen and hydrogen atoms of water in the direction (*z*) normal to (A,B) the graphene sheet, or (C,D) the monolayer BN sheet.

average is nonzero but slightly negative. This net negative charge will induce a counter-charge at the contacting surface of the graphene sheet. For our droplet−graphene system, the fitted total positive charges on the contacting surface of graphene are about 1.3*e* based on DFT calculation (*via* integration of the calculated electron density). To our knowledge, the phenomenon of water-induced charge on the contacting surface of graphene has not been reported in the literature. The classical MD simulation cannot predict such surface charges unless a polarizable model for the graphene carbon atoms is employed. Our DFT calculation of the surface charge can provide a benchmark test for the polarizable carbon model.

Unlike carbon atoms, boron and nitrogen atoms exhibit opposite charges. Hence, the density distributions of oxygen and hydrogen atoms on top of the BN sheet will be very different from those on the graphene. As shown in Figure 4C, because the boron atoms possess positive charges, which tend to attract more oxygen atoms nearby, the first oxygen peak (calculated from boron-based cylinders) is much higher than the hydrogen peak. On the other hand, the first hydrogen peak (calculated from nitrogen-based cylinders) is much higher than the first oxygen peak (see Figure 4D). Overall, there are ~1.2*e* net positive charges on the contacting surface of BN sheet based on the DFT calculation.

The orientation distributions of water molecules, computed based on the angle (φ) between an OH bond of water molecules and the *z* axis, can also exhibit the layered microstructure for droplet near the substrate. According to a previous study,[52] interfacial water molecules can be divided into three groups: (1) those with the "dangling" (**D**) OHs which point toward the substrate and lying next to the substrate, (2) those with the "tangent" (**T**) OHs which are nearly parallel to substrate, and (3) those with the "bulk" (**B**) OHs which point away from the substrate. The orientation state can then be distinguished by the angle with respect to the normal vector (*z* axis), namely, 150−180° for the **D** state, 70−120° for the **T** state, and 0−20° for the **B** state. In Figure 5, we show that most of the water molecules in the first water layer next to the substrate adopt **T** orientation in all three systems. It is known that water molecules tend to adopt parallel positions near a hydrophobic substrate, while near a hydrophilic substrate, most water molecules tend to adopt the orientation with one OH pointing toward the substrate. Here, the orientation distributions of water molecules in the first water layer are nearly the same in all three systems, about 5%, 50%, and 5% molecules in the **D**, **T**, and **B** states, respectively. Thus, our QMD simulations show that both graphene and BN sheets are hydrophobic. In the second water layer next to the substrate, most water molecules still adopt the **T** orientation. It is worthy of noting that in the first water layer, the

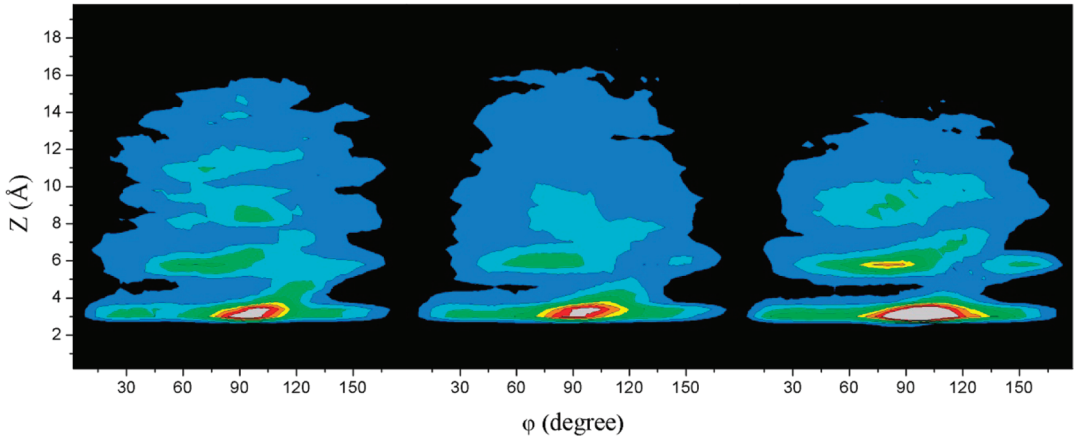

Figure 5. Distance–orientation distribution of water OH bonds as a function of the distance z and the angle φ in three systems: (A) W125-C-298K, (B) W125-C-385K, and (C) W125-BN-385K, respectively. Color code: Gray, red, yellow, green, light blue, dark blue, and black are in the order of high to zero probability distribution.

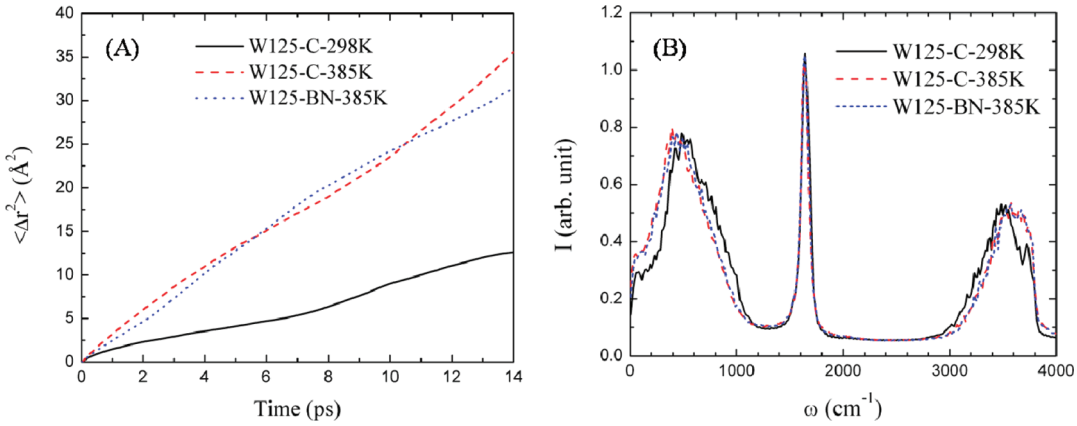

Figure 6. (A) Mean square displacements of water molecules on the graphene sheet at 298 or 385 K, or on BN sheet at 385 K. The origin (or 0 ps) in the time axis can be any time in the QMD simulation after the system reaches thermal equilibrium (typically after 10 ps). (B) Calculated vibration spectra of water molecules in the three systems based on the Fourier transform of velocity autocorrelation functions.

maximum distribution centers around $\varphi \approx 110°$, indicating that the OHs slightly point away from the bulk. This state can be referred to as the clathrate **T** orientation. However, in the second water layer, most OHs slightly point toward the droplet with the maximum distribution being around $\varphi \approx 80°$. This state can be referred to as the anticlathrate **T** orientation. There are also small peaks corresponding to OHs adopting the **D** orientation in the second water layer. In the systems of droplet–graphene at 298 K and droplet-BN at 385 K, the third water layer near the substrate can be also distinguished, with most water molecules still lying parallel to the substrate. However, in the droplet–graphene system at 385 K, the water beyond the second water layer behaves like the bulk, where the orientation of water molecules is fairly random. It should be mentioned that, for the classical model systems shown in Figure 3, the interfacial water molecules adopt the **T** orientation near the flat BN sheet, whereas most water molecules adopt the **D** orientation near the wrinkled BN sheet.

Diffusive Property, Vibration Spectra of Water. To investigate diffusivity of water molecules in the nanodroplets, we calculate the mean square displacement (MSD) of the oxygen atoms (Figure 6A). According to the Einstein relation, the self-diffusion constant (D) can be calculated from the slope of MSD–time curve. The water droplets at 385 K have nearly the same self-diffusion constant for both droplet–graphene ($D = 4.0 \times 10^{-5}$ cm^2/s) and droplet–BN ($D = 3.7 \times 10^{-5}$ cm^2/s) systems, in excellent agreement with the experimental value ($D = 2.4 \times 10^{-5}$ cm^2/s) for the bulk water in the ambient condition. The diffusion constant for the droplet–graphene system at 298 K ($D = 1.5 \times 10^{-5}$ cm^2/s) is smaller than that at 385 K, indicating that although the supercooled water has appreciably lower diffusivity than the ambient water it is still considerably higher than that of bulk ice whose diffusion constant is typically on the order of 10^{-9} cm^2/s.[53]

In addition, the Fourier transform of velocity autocorrelation functions gives rise to vibration spectra of water molecules (see Figure 6B). Three major peaks can

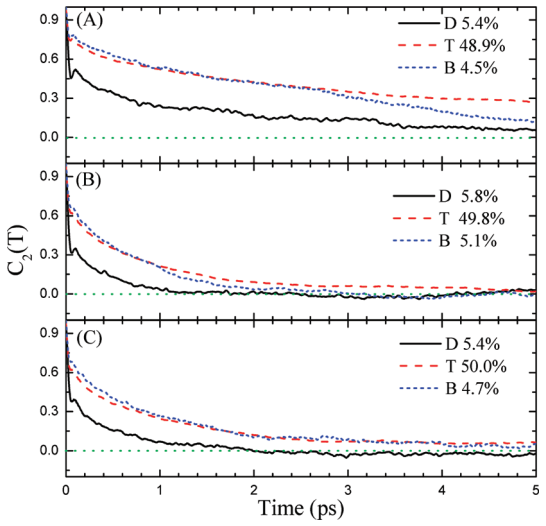

Figure 7. Second-order orientation time-correlation function $C_2(t)$ of the interfacial water OHs in the dangling (D), tangent (T), and pointing to the bulk (B) states for the system (A) W125-C-298K, (B) W125-C-385K, and (C) W125-BN-385K, respectively. The relative populations of these three states are also listed in the legend.

be seen in the frequency range of 0−4000 cm^{-1}, where the broad peak in the range of 3000−4000 cm^{-1} corresponds to the OH bond stretching mode, the sharp peak at ∼1600 cm^{-1} corresponds to H−O−H bending mode, and the broad peak in the range of 0−1000 cm^{-1} corresponds to intermolecular vibration. The peak position and the shape of vibration spectra are weakly dependent on the temperature. The peak of intermolecular vibration is red-shifted, while the peak of OH bond stretching is blue-shifted from 298 to 385 K, indicating that the intermolecular hydrogen bonds become weaker with increasing temperature. However, the nearly perfect superposition of the spectra for the droplet−graphene and droplet−BN systems suggests that the vibration spectra are little affected by the substrate as long as the nanodroplet is sufficiently large.

The reorientation dynamics of the **D**, **T**, and **B** states can be used to characterize dynamic properties of water near the substrate. Water reorientation can be expressed by the second-order Legendre polynomial of the time-correlation function

$$C_2(t) = \langle P_2[\vec{u}(0)\cdot\vec{u}(t)]\rangle \quad (1)$$

where $\vec{u}(t)$ designates the orientation of the water OH bond at time t. Figure 7 shows the decay of $C_2(t)$ of the interfacial water in the **D**, **T**, and **B** state, computed from the QMD simulations. It can be seen that the decay of $C_2(t)$ of the **D** state is much faster than that of the **T** and **B** states, consistent with the classic MD simulation.[54] The decay of $C_2(t)$ can be fitted to a single-exponential function

$$C_2(t) = e^{-t/\tau_{rot}} \quad (2)$$

which has been previously reported in ultrafast IR spectroscopy measurment[55,56] and classic MD simulations. Here, τ_{rot} is the time constant of the decay. It has been shown that the SPC/E model gives τ_{rot} = 2.5 ps for the bulk water in the ambient condition, but the tangent (**T**) state of water in the first molecular layer next to a hydrophobic substrate has a much slower reorientation rate, with τ_{rot} = 4.8 ps.[52] The τ_{rot} measured from NMR is 1.5−2.5 ps for the water in contact to hydrophobic peptides and hydrophobic patch of protein.[56,57] In the present QMD simulations, τ_{rot} of the **T** state is 3.0 and 1.0 ps at 298 and 385 K, respectively. The latter value is in good agreement with the NMR measurements.

CONCLUSIONS

We have performed quantum molecular dynamics simulation to the study wetting process of water nanodroplets in contact with a graphene or monolayer BN sheet. To account for the intermolecular van der Waals interactions, Grimme dispersion correction is included in the QMD simulations. Our QMD simulations show that both graphene and monolayer BN sheets are weakly hydrophobic with nearly the same contact angles for water (87° and 86°, respectively). For water droplets in a supercooled state and in contact with graphene, the contact angle becomes appreciably larger (∼96°). Although the monolayer BN sheets entail large local dipole moments, our QMD simulation shows that the atomically flat BN sheets are still hydrophobic due to the lack of a net dipole normal to the sheet. In real experimental conditions, however, most monolayer BN sheets may not be perfectly flat and may contain defects. As a result, local dipoles normal to the BN sheets arise, which could render the BN sheets apparently much more hydrophilic (*i.e.*, having much higher wettability).

The different distributions of O and H atoms near the graphene or BN sheets result in a net electric field at the substrate-droplet interfaces. Our QMD simulations show that the water nanodroplet (with 125 molecules) yields 1.3*e* charges on the contacting surface of the graphene, and 1.2*e* charges on the contacting surface of the BN sheet. In view that graphene is a semimetal with a zero electronic band gap, such charge induction may affect electronic structure of the contacting graphene. The calculated orientation distributions show that on a graphene or BN sheet, most water molecules in the first molecular layer next to the substrate tend to adopt tangent orientation, while the second and the third molecular layers exhibit similar tendency for the water orientation, but less distinguishable.

The calculated diffusion constant of water from the QMD simulation is in very good agreement with the experimentally measured value for the bulk water in

the ambient condition. As expected, the diffusion constant of supercooled water is notably smaller than that of the ambient water. The calculated IR vibration spectra show that the vibration of water molecules in the nanodroplets is little affected by the substrate. However, in the supercooled state, the intermolecular H-bond band is blue-shifted, and the O–H bond stretching band is red-shifted. Finally, the reorientation dynamics of OH bonds of interfacial water molecules are investigated with the rotation time constant calculated based on the time-correlation function and are found to be very close to the experimental value.

COMPUTATIONAL MODEL AND METHODS

In the Born–Oppenheimer QMD simulations, the water nanodroplet with 125 water molecules, initially in cubic shape, is located in contact with a rectangular 12 × 7 unit cells of graphene or monolayer BN sheet. Either the graphene or the BN sheet is composed of 336 atoms. The spatial dimensions of the simulation supercell are about 30 Å × 30 Å × 30 Å, which are large enough to neglect the interactions between the substrate/droplet and their periodic images. The water nanodroplet is first optimized using a density-functional theory (DFT) method before the QMD simulations. The graphene and BN sheets are fixed in the *xy* plane during the QMD simulations.

Specifically, the QMD simulations are performed using the DFT method with the Becke–Lee–Yang–Parr (BLYP)[58,59] exchange-correlation functional. The Goedecker–Teter–Hutter (GTH)[60,61] norm-conserved pseudopotentials are used for the description of the core electrons, and the GTH-DZVP Gaussian basis[62] together with a plane-wave basis set (with an energy cutoff of 280 Ry) are chosen to expand electronic wave functions. It is well-known that the generalized-gradient approximation (GGA) functionals like BLYP generally underestimate the intermolecular dispersion interaction. Hence, the Grimme's van der Waals correction[63,64] is included in the QMD simulations to account for the dispersion interaction more accurately. The QMD simulations are performed in the constant volume and constant temperature (*NVT*) ensemble. The Nose–Hoover–Chain coupling method is used to control the temperature.

The freezing temperatures of bulk water have been computed by Yoo *et al.*[65] based on QMD simulations. It has been found that the two commonly used GGA functionals, Perdew–Burke–Ernzerhof (PBE)[66] and BLYP, give the freezing temperatures of 417 and 411 K, respectively. By including the Grimme van der Waals correction in the BLYP-D (BLYP plus dispersion) functional, the computed freezing temperature becomes 360 K,[67] still much higher than 273 K of real water. Hence, to mimic real water nanodroplet in the ambient condition, the 385 K temperature is chosen for the QMD simulations.

In total, three independent QMD simulations have been carried out, namely, a water nanodroplet on the graphene sheet at 298 K (denoted as W125-C-298K), a water nanodroplet on the graphene sheet at 385 K (W125-C-385K), and a water nanodroplet on the BN sheet at 385 K (W125-BN-385K). The time step is 1.0 fs, and the total simulation time for each system ranges from 24 to 30 ps. The QUICKSTEP program implemented in the CP2K package is used for the QMD simulations.[68,69]

Conflict of Interest: The authors declare no competing financial interest.

Acknowledgment. This work is supported by grants from the NSF (Grants CBET-1036171 and CBET-1066947), ARL (Grant W911NF1020099), and a grant from Nebraska Center for Energy Sciences Research, and by the University of Nebraska's Holland Computing Center.

Supporting Information Available: Movies of water nanodroplets in contact with the graphene sheet. This material is available free of charge *via* the Internet at http://pubs.acs.org.

REFERENCES AND NOTES

1. Giovambattista, N.; Debenedetti, P. G.; Rossky, P. J. Effect of Surface Polarity on Water Contact Angle and Interfacial Hydration Structure. *J. Phys. Chem. B* **2007**, *111*, 9581–9587.
2. Sposito, G.; Skipper, N. T.; Sutton, R.; Park, S.-H.; Scoper, A. K.; Greathoouse, J. A. Surface Geochemistry of the Clay Minerals. *Proc. Natl. Acad. Sci.* **1999**, *96*, 3358–3364.
3. Leng, Y.; Cummings, P. T. Fluidity of Hydration Layers Nanoconfined between Mica Surfaces. *Phys. Rev. Lett.* **2005**, *94*, 026101.
4. Tanford, C. *The Hydrophobic Effect: Formation of Micelles and Biological Membranes*, 2nd ed.; Wiley: New York, 1980.
5. Kauzmann, W. Some Factors in the Interpretation of Protein Denaturation. *Adv. Protein Chem.* **1959**, *14*, 1–63.
6. Dill, K. A. Dominant Forces in Protein Folding. *Biochemistry* **1990**, *29*, 7133–7155.
7. Chandler, D. Interfaces and the Driving Force of Hydrophobic Assembly. *Nature* **2005**, *437*, 640–647.
8. Luna, M.; Colchero, J.; Baró, A. M. Study of Water Droplets and Films on Graphite by Noncontact Scanning Force Microscopy. *J. Phys. Chem. B* **1999**, *103*, 9576–9581.
9. Gil, A.; Colchero, J.; Luna, M.; Gómez-Herrero, J.; Baró, A. M. Adsorption of Water on Solid Surfaces Studied by Scanning Force Microscopy. *Langmuir* **2000**, *16*, 5086–5092.
10. Adamson, A. W.; Gast, A. P. *Physical Chemisry of Surfaces*, 6th ed.; John Wiley & Sons: New York, 1997.
11. Liu, J.; Rinzler, A. G.; Dai, H.; Hafner, J. H.; Bradley, R. K.; Boul, P. J.; Lu, A.; Iverson, T.; Shelimov, K.; Huffman, C. B.; *et al.* Fullerene Pipes. *Science* **1998**, *280*, 1253–1256.
12. Rieutord, F.; Salmeron, M. Wetting Properties at the Submicrometer Scale: A Scanning Polarization Force Microscopy Study. *J. Phys. Chem. B* **1998**, *102*, 3941–3944.
13. Noca, F.; Hoenk, M.; Hunt, B.; Koumoutsakos, P.; Walther, J.; Werder, T. Bio-inspired Acoustic Sensors Based on Artificial Stereocilia. *J. Acoust. Soc. Am.* **2000**, *108*, 2494.
14. Liu, H.; Zhaia, J.; Jiang, L. Wetting and Anti-wetting on Aligned Carbon Nanotube Films. *Soft Matter* **2006**, *2*, 811–821.
15. Shin, Y. J.; Wang, Y.; Huang, H.; Kalon, G.; Wee, A. T. S.; Shen., Z; Bhatia, C. S.; Yang, H. Surface-Energy Engineering of Graphene. *Langmuir* **2010**, *26*, 3798–3802.
16. Wang, S.; Zhang, Y.; Abidi, N.; Cabrales, L. Wettability and Surface Free Energy of Graphene Films. *Langmuir* **2009**, *25*, 11078–11081.
17. Werder, T.; Walther, J. H.; Jaffe, R. L.; Halicioglu, T.; Koumoutsakos, P. On the Water–Carbon Interaction for Use in Molecular Dynamics Simulations of Graphite and Carbon Nanotubes. *J. Phys. Chem. B* **2003**, *107*, 1345–1352.
18. Cicero, G.; Grossman, J. C.; Schwegler, E.; Gygi, F.; Galli, G. Water Confined in Nanotubes and between Graphene Sheets: A First Principle Study. *J. Am. Chem. Soc.* **2008**, *130*, 1871–1878.
19. Werder, T.; Walther, J. H.; Jaffe, R. L.; Halicioglu, T.; Noca, F.; Koumoutsakos, P. Molecular Dynamics Simulation of Contact Angles of Water Droplets in Carbon Nanotubes. *Nano Lett.* **2001**, *1*, 697–702.
20. Leenaerts, O.; Partoens, B.; Peeters, F. M. Water on Graphene: Hydrophobicity and Dipole Moment Using Density Functional Theory. *Phys. Rev. B* **2009**, *79*, 235440.

21. Koishi, T.; Yasuoka, K.; Fujikawa, S.; Ebisuzaki, T.; Zeng, X. C. Coexistence and Transition between Cassie and Wenzel State on Pillared Hydrophobic Surface. *Proc. Natl. Acad. Sci.* **2009**, *106*, 8435–8440.
22. Meng, S.; Zhang, Z.; Kaxiras, E. Tuning Solid Surfaces from Hydrophobic to Superhydrophilic by Submonolayer Surface Modification. *Phys. Rev. Lett.* **2006**, *97*, 036107.
23. Zhang, X.; Zhu, Y.; Granick, S. Hydrophobicity at a Janus Interface. *Science* **2002**, *295*, 663–666.
24. Ge, Z.; Cahill, D. C.; Braun, P. V. Thermal Conductance of Hydrophilic and Hydrophobic Interfaces. *Phys. Rev. Lett.* **2006**, *96*, 186101.
25. Koishi, T.; Yasuoka, K.; Ebisuzaki, T.; Yoo, S.; Cheng, X. C. Large-Scale Molecular-Dynamics Simulation of Nanoscale Hydrophobic Interaction and Nanobubble Formation. *J. Chem. Phys.* **2005**, *123*, 204707.
26. Giovambattista, N.; Debenedetti, P. G.; Rossky, P. J. Hydration Behavior under Confinement by Nanoscale Surfaces with Patterned Hydrophobicity and Hydrophilicity. *J. Phys. Chem. C* **2007**, *111*, 1323–1332.
27. Cieplak, M.; Koplik, J.; Banavar, J. R. Nanoscale Fluid Flows in the Vicinity of Patterned Surfaces. *Phys. Rev. Lett.* **2006**, *96*, 114502.
28. Cheng, Y.-K.; Rossky, P. J. The Effect of Vicinal Polar and Charged Groups on Hydrophobic Hydration. *Biopolymers* **1999**, *50*, 742–750.
29. Rowlinson, J. S.; Widom, B. *Molecular Theory of Capillarity*; Oxford University Press: Oxford, 1982.
30. de Gennes, P.-G.; Brochard-Wyart, F.; Quéré, D. *Capillarity and Wetting Phenomena: Drops, Bubbles, Pearls, Waves*; Springer Science + Business Media, Inc.: New York, 2004.
31. Bico, J.; Marzolin, C.; Quéré, D. Pearl Drops. *Europhys. Lett.* **1999**, *47*, 220–226.
32. Lafuma, A.; Quéré, D. Superhydrophobic States. *Nat. Mater.* **2003**, *2*, 457–460.
33. Yang, C.; Tartaglino, U.; Persson, B. N. J. Influence of Surface Roughness on Superhydrophobicity. *Phys. Rev. Lett.* **2006**, *97*, 116103.
34. Feng, L.; Li, S.; Li, Y.; Li, H.; Zhang, L.; Zhai, J.; Song, Y.; Liu, B.; Jiang, L.; Zhu, D. Super-hydrophobic Surfaces: From Natural to Artificial. *Adv. Mater.* **2002**, *14*, 1857–1860.
35. Li, G.-X.; Liu, Y.; Wang, B.; Song, X.-M.; Li, E.; Yan, H. Preparation of Transparent BN Films with Superhydrophobic Surface. *Appl. Surf. Sci.* **2008**, *254*, 5299–5303.
36. Lee, C. H.; Drelich, J.; Yap, Y. K. Superhydrophobicity of Boron Nitride Nanotubes Grown on Silicon Substrates. *Langmuir* **2009**, *25*, 4853–4860.
37. Stillinger, F. H. Concluding Remarks for FD 146: Answers and Questions. *Faraday Discuss* **2010**, *146*, 395–401.
38. Rahman, A.; Stillinger, F. H. Molecular Dynamics Study of Liquid Water. *J. Chem. Phys.* **1971**, *55*, 3336–3359.
39. Berendsen, H. J. C.; Grigera, J. R.; Straatsma, T. P. The Missing Term in Effective Pair Potentials. *J. Phys. Chem.* **1987**, *91*, 6269–6271.
40. Jorgensen, W. L. Quantum and Statistical Mechanical Studies of Liquids. 10. Transferable Intermolecular Potential Functions for Water, Alcohols, and Ethers. Application to liquid water. *J. Am. Chem. Soc.* **1981**, *103*, 335–340.
41. Jorgensen, W. L.; Chandrasekhar, J.; Madura, J. D.; Impey, R. W.; Klein, M. L. Comparison of Simple Potential Functions for Simulating Liquid Water. *J. Chem. Phys.* **1983**, *79*, 926.
42. Mahoney, M. W.; Jorgensen, W. L. A Five-Site Model for Liquid Water and the Reproduction of the Density Anomaly by Rigid, Nonpolarizable Potential Functions. *J. Chem. Phys.* **2000**, *112*, 8910.
43. Pertsin, A.; Grunze, M. Water–Graphite Interaction and Behavior of Water Near the Graphite Surface. *J. Phys. Chem. B* **2004**, *108*, 1357–1364.
44. Stillinger, F. H. J. Structure in Aqueous Solutions of Nonpolar Solutes from the Standpoint of Scaled-Particle Theory. *Solution Chem.* **1973**, *2*, 141–158.
45. Lum, K.; Chandler, D.; Weeks, J. D. Hydrophobicity at Small and Large Length Scales. *J. Phys. Chem. B* **1999**, *103*, 4570–4577.
46. Lum, K.; Luzar, A. Pathway to Surface-Induced Phase Transition of a Confined Fluid. *Phys. Rev. E* **1997**, *56*, 6283–6286.
47. Truskett, T. M.; Debenedetti, P. G.; Torquato, S. Thermodynamic Implications of Confinement for a Waterlike Fluid. *J. Chem. Phys.* **2001**, *114*, 2401.
48. Choudhury, N.; Pettitt, B. M. On the Mechanism of Hydrophobic Association of Nanoscopic Solutes. *J. Am. Chem. Soc.* **2005**, *127*, 3556–3567.
49. Koishi, T.; Yoo, S.; Yasuoka, K.; Zeng, X. C.; Narumi, T.; Susukita, R.; Kawai, A.; Furusawa, H.; Suenaga, A.; Okimoto, N.; *et al.* Nanoscale Hydrophobic Interaction and Nanobubble Nucleation. *Phys. Rev. Lett.* **2004**, *93*, 185701.
50. Huang, X.; Margulis, C. J.; Berne, B. J. Dewetting-Induced Collapse of Hydrophobic Particles. *Proc. Natl. Acad. Sci. U.S.A.* **2003**, *100*, 11953–11958.
51. Hummer, G.; Rasaiah, J. C.; Noworyta, J. P. Water Conduction through the Hydrophobic Channel of a Carbon Nanotube. *Nature* **2001**, *414*, 188–190.
52. Stirnemann, G.; Rossky, P. J.; Hynes, J. T.; Laage, D. Water Reorientation, Hydrogen-Bond Dynamics and 2D-IR Spectroscopy Next to an Extended Hydrophobic Surface. *Faraday Discuss* **2010**, *146*, 263–281.
53. Koga, K.; Tanaka, H.; Zeng, X. C. First-Order Transition in Confined Water between High-Density Liquid and Low-Density Amorphous Phases. *Nature* **2000**, *408*, 564–567.
54. Rezus, Y. L. A.; Bakker, H. J. On the Orientational Relaxation of HDO in Liquid Water. *J. Chem. Phys.* **2005**, *123*, 114502.
55. Park, S.; Moilanen, D. E.; Fayer, M. D. Water Dynamics—The Effects of Ions and Nanoconfinement. *J. Phys. Chem. B* **2008**, *112*, 5279–5290.
56. Qvist, J.; Halle, B. Thermal Signature of Hydrophobic Hydration Dynamics. *J. Am. Chem. Soc.* **2008**, *130*, 10345–103530.
57. Mattea, C.; Qvist, J.; Halle, B. Dynamics at the Protein–Water Interface from ^{17}O Spin Relaxation in Deeply Supercooled Solutions. *Biophys. J.* **2008**, *95*, 2951–2963.
58. Becke, A. D. Density-Functional Exchange-Energy Approximation with Correct Asymptotic Behavior. *Phys. Rev. A* **1988**, *38*, 3098–3100.
59. Lee, C.; Yang, W.; Parr, R. G. Development of the Colle–Salvetti Correlation-Energy Formula into a Functional of the Electron Density. *Phys. Rev. B* **1988**, *37*, 785–789.
60. Goedecker, S.; Teter, M.; Hutter, J. Separable Dual-Space Gaussian Pseudopotentials. *Phys. Rev. B: Condens. Matter.* **1996**, *54*, 1703–1710.
61. Hartwigsen, C.; Goedecker, S.; Hutter, J. Relativistic Separable Dual-Space Gaussian Pseudopotentials from H to Rn. *Phys. Rev. B: Condens. Matter.* **1998**, *58*, 3641–3662.
62. VandeVondele, J.; Hutter, J. Gaussian Basis Sets for Accurate Calculations on Molecular Systems in Gas and Condensed Phases. *J. Chem. Phys.* **2007**, *127*, 114105.
63. Grimme, S. Accurate Description of Van der Waals Complexes by Density Functional Theory Including Empirical Corrections. *J. Comput. Chem.* **2004**, *25*, 1463–1473.
64. Grimme, S. Semiempirical GGA-Type Density Functional Constructed with a Long-Range Dispersion Correction. *J. Comput. Chem.* **2006**, *27*, 1787–1799.
65. Yoo, S.; Zeng, X. C.; Xantheas, S. S. On the Phase Diagram of Water with Density Functional Theory Potentials: The Melting Temperature of Ice I_h with the Perdew–Burke–Ernzerhof and Becke–Lee–Yang–Parr Functional. *J. Chem. Phys.* **2009**, *130*, 221102.
66. Perdew, J. P.; Burke, K.; Ernzerhof, M. Generalized Gradient Approximation Made Simple. *Phys. Rev. Lett.* **1996**, *77*, 3865.
67. Yoo, S.; Xantheas, S. S. The Effect of Dispersion Corrections on the Melting Temperature of Liquid Water. *J. Chem. Phys.* **2011**, *134*, 121105.
68. VandeVondele, J.; Krack, M.; Mohamed, F.; Parrinello, M.; Chassaing, T.; Hutter, J. Quickstep: Fast and Accurate Density Functional Calculations Using a Mixed Gaussian and Plane Waves Approach. *Comput. Phys. Commun.* **2005**, *167*, 103–128.
69. Lippert, G.; Hutter, J.; Parrinello, M. A Hybrid Gaussian and Plane Wave Density Functional Scheme. *Mol. Phys.* **1997**, *92*, 477–488.